Bull. Natl. Mus. Nat. Sci., Ser. C, 38, pp. 15–32, December 22, 2012

LA-ICP-MS and SHRIMP ages of zircons in chevkinite and monazite tuffs from the Boso Peninsula, Central Japan

Yukiyasu Tsutsumi[1], Kenji Horie[2], Takashi Sano[1], Ritsuro Miyawaki[1], Koichi Momma[1], Satoshi Matsubara[1], Masako Shigeoka[1] and Kazumi Yokoyama[1]*

[1] Department of Geology and Paleontology, National Museum of Nature and Science, 4–1–1 Amakubo, Tsukuba, Ibaraki 305–0005, Japan
*Author for correspondence: ytsutsu@kahaku.go.jp
[2] National Institute of Polar Research, 10–3 Midori-cho, Tachikawa, Tokyo 190–8518, Japan

Abstract Specific tuffs including chevkinite and monazite were found in Oligocene to Miocene formations on the Boso Peninsula in central Japan. In the Japanese Islands, chevkinite is found only in a granitoid, whereas monazite is found more commonly in granitoids, high-grade metamorphic rocks and sandstone. The occurrence of monazite as phenocrysts found in tuff is the first observations in the islands. Chevkinite was found in a greenish tuff in Hegurinaka quarry. Monazite was found in the tuffs at both the Hegurinaka and Shirataki areas of the Boso Peninsula. Ages of the tuffs were obtained from coexisting zircons by Laser Ablation Inductively Coupled Plasma Mass Spectrometry (LA-ICP-MS) and Sensitive High Resolution Ion Microscopy (SHRIMP). The SHRIMP age of the chevkinite-bearing tuff from Hegurinaka is 22.9 ± 0.1 Ma. The LA-ICP-MS age of the monazite tuff from Shirataki is 22.2 ± 1.5 Ma similar to the LA-ICP-MS age of the chevkinite tuff, 22.1 ± 0.8 Ma. Volcanic activity from 20 Ma to 25 Ma occurred mostly along the coast of the Sea of Japan. Detrital monazite with an age of more than 1800 Ma in the Hegurinaka chevkinite tuff shows that it was derived from the continental side, i.e. the present Japanese Islands or the Asian continent. Hence, it is probable that the specific tuffs were derived from the area around the present Sea of Japan just before opening.

Key words: chevkinite, LA-ICP-MS, SHRIMP, zircon, monazite

Introduction

Chevkinite, $(Ce,La,Ca)_4(Fe^{2+},Mg)_2(Ti,Fe^{3+})_3Si_4O_{22}$, is a rare mineral occurring as an accessory mineral in granitoid, pegmatite, and air-fall ash deposits (Michell, 1966; Izett *et al.*, 1968; Sokolova *et al.*, 2004; Platt *et al.*, 1987; Macdonald *et al.*, 2012). In the Japanese Islands, chevkinite has only been found in a Middle Miocene granitoid from Cape Ashizuri on Shikoku Island (Imaoka and Nakashima, 1994). Monazite, $(Ce,La,Nd,Th)PO_4$, occurs mostly as an accessory mineral in granitoid and high-grade metamorphic rock, and it is rarely found in a tuff (Das *et al.*, 2009). Recently, monazite has become one of the most important minerals for age analyses and provenance studies because it is commonly found as detrital grains in river and beach sands and in sandstone (e.g. Yokoyama *et al.*, 2010).

Neither of these (Rare Earth Element) REE minerals has been reported previously in volcanic rocks on the Japanese Islands. In this paper, we describe tuffs with chevkinite and monazite phenocrysts that were found on the Boso Peninsula of Honshu Island in Japan, and we discuss the analyzed chemical compositions of the minerals and ages of the tuffs through Electron Probe Micro-analysis (EPMA), Sensitive High Resolution Ion Microscopy (SHRIMP), and Laser Ablation Inductively Coupled Plasma Mass Spectrometry (LA-ICP-MS).

Geological setting

The Boso Peninsula consists mainly of the

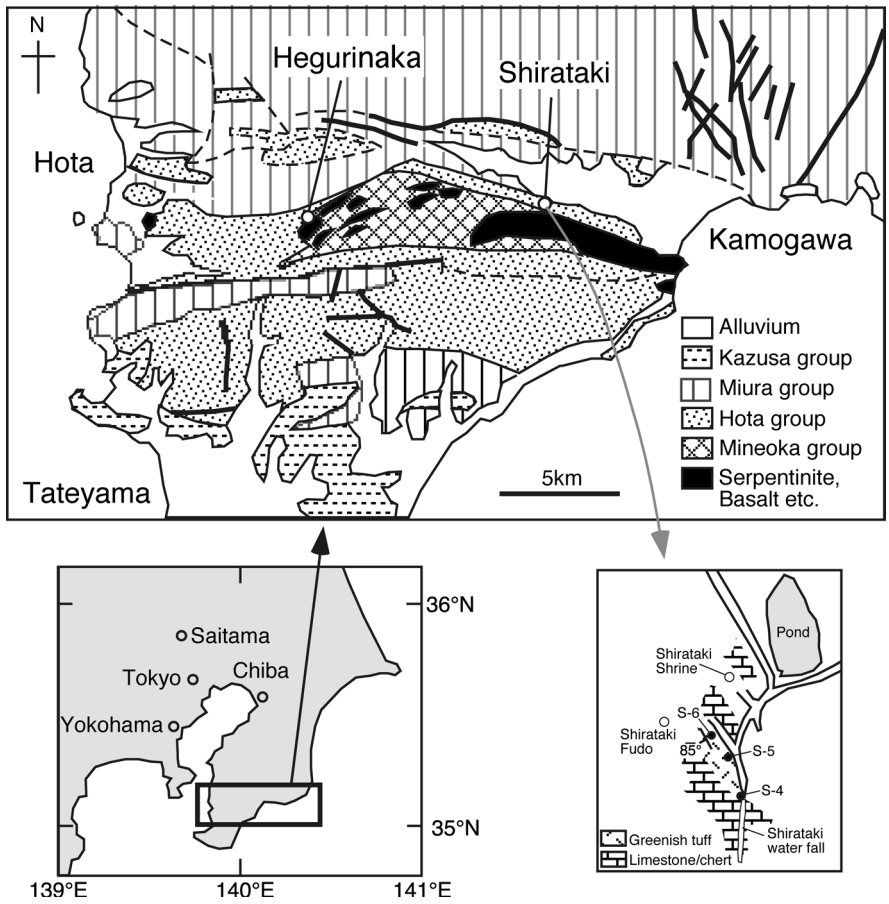

Fig. 1. Simplified geological map of the central part of the Boso Peninsula with sample localities at the Shirataki area.

Middle Miocene to Quaternary volcaniclastic sequence Miura and Kazusa groups (Mitsunashi *et al.*, 1978). Peridotite (mostly in the form of serpentinite), gabbro, and basalt occur at the southern part of the peninsula (Fig. 1), and are considered to be a part of an ophiolite sequence. Pelagic sediments such as limestone and chert occur locally and are associated with basaltic rock. They are also a member of the ophiolite sequence and occur discontinuously along serpentinite bodies with an east-west trend. Basic schist was found at the eastern end of the peninsula but has no clear contact relationships with serpentinite because of a poor exposure, although it is probably a member of the sequence. All these rocks occur as tectonic blocks and are associated with sandstone and shale. Both the ophiolite sequence and the sedimentary rocks belong to a member of the Mineoka Belt. The belt is mostly in fault contact with the early Miocene volcaniclastic sequence the Hota Group. The ophiolite sequence and sedimentary rocks continue to the northwest and are treated as a part of the eastern end of the Shimanto Belt, which is composed totally of a subduction complex. Many microfossil ages and isotope ages were determined from the constituents of the Mineoka Belt. K-Ar ages of the igneous and metamorphic rocks range from 14 Ma to 94 Ma (e.g. Yoshida, 1974; Hiroi, 1995; Saito, 1992). Microfossils in the sedimentary rocks such as limestone, chert, and siliceous shale range from Eocene to Early Mio-

cene. It is not still clear whether each block belongs to a member of the sedimentary rocks of the Shimanto Group, an ophiolite sequence, or a later stage volcaniclastic sequence.

Greenish tuffs occur in the tectonic block at the Hegurinaka quarry and the Shirataki area. Both of these locations were discussed in detail by many authors (e.g. Saito, 1992; Takahashi, 1994; Mohiuddin and Ogawa, 1996, 1998 a and b; Hirano *et al.*, 2003). In the Shirataki area, a greenish tuff apparently occurs within the limestone-chert sequence (Fig. 1). Saito (1992) summarized data of planktonic foraminifers, radioralian fossils, and calcareous nannofossils and concluded that the limestone-chert sequence belongs to the Middle to Upper Eocene. On the other hand, Mohiuddin and Ogawa (1998a) found planktonic foraminifers with an age from the Early Miocene. There is no direct contact between the limestone-chert and tuff.

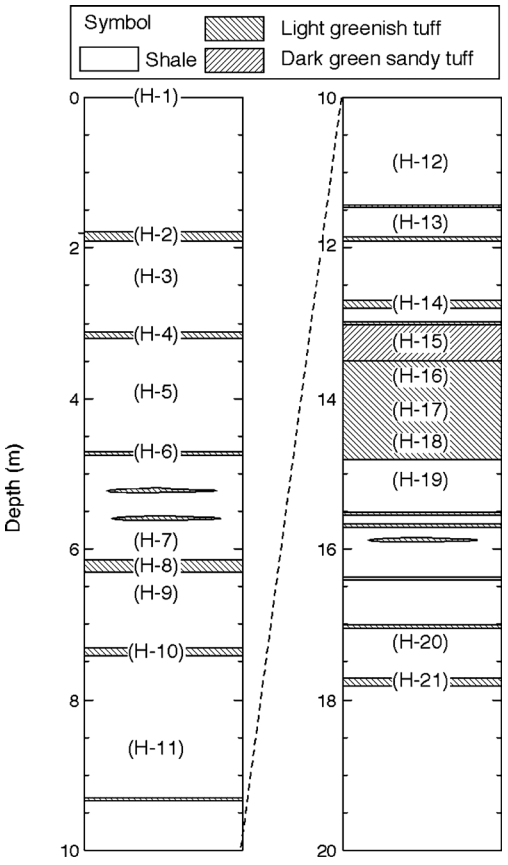

Fig. 2. Columnar section of the shale-tuff sequence at the Hegurinaka quarry.

In the Hegurinaka quarry, several tuff layers occur intercalated with shale (Fig. 2). Takahashi (1994) described these rocks as a glauconite-rich shale zone. A limestone-chert sequence and basaltic rock occur below the shale-tuff sequence. Mohiuddin and Ogawa (1996, 1998b) studied planktonic foraminifers in the limestone-chert sequence and obtained an age from the Early Eocene to Middle Miocene. Unfortunately, the limestone-chert sequence had been excavated and was no longer exposed. Radioralian fossils from the shale-tuff sequence show the earliest Miocene ages or show the boundary between the Oligocene and Miocene (Saito, 1992). Whole rock Ar–Ar age data of the basalt was obtained by Hirano *et al.* (2003). The age was determined to be 19.6 ± 0.9, Early Miocene. In the shale-tuff sequence, a tuff layer is more than 1 meter in thickness and usually greenish in color (Fig. 3A). The other tuff layers are also mostly greenish, but less than 20 cm in thickness. Dark green sandy tuff occurs above the thick greenish tuff (Figs. 2 and 3A).

Description of tuffs

In the Shirataki area, three greenish tuff samples were collected. S-4 tuff occurring along a stream is a grassy tuff, depleted in crystal fragments (Fig. 3B). S-5 tuff is rich in fragments (Fig. 3C). S-6 tuff contains a moderate amount of fragments. Under microscopic observation, crystal fragments are mostly quartz and plagioclase. Mafic minerals except for biotite have been totally replaced or resolved. Ilmenite is partly replaced by anatase. Grassy parts of all the tuffs are totally altered into clay minerals. A calcite vein develops locally in most of the tuff samples. As an accessory mineral, zircon and monazite occur. They are usually ultrastable minerals and are treated as magmatic in origin. Glauconite, chlorite, pyrite, and galena are found as secondary minerals. Both zircon and monazite are

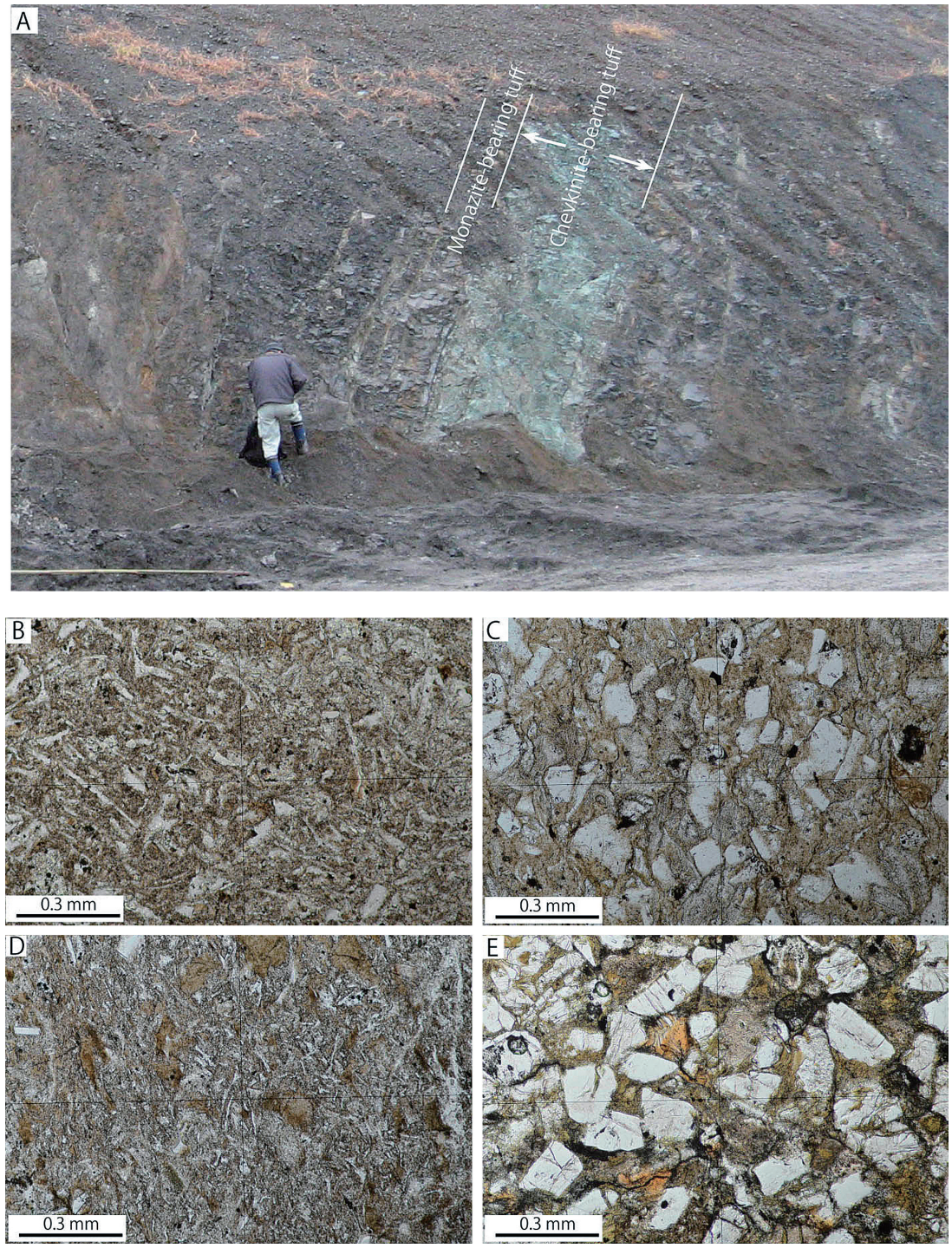

Fig. 3. Outcrop, A, of the thick greenish tuff at the Hegurinaka quarry and photomicrographs of the tuffs from Hegurinaka and Shirataki. B: grassy tuff, S-4, from Shirataki. C: fragment-rich tuff, S-5, Shirataki. D: grassy tuff, H-16, from Hegurinaka. F: fragment-rich sandy tuff, H-15, from the Hegurinaka quarry.

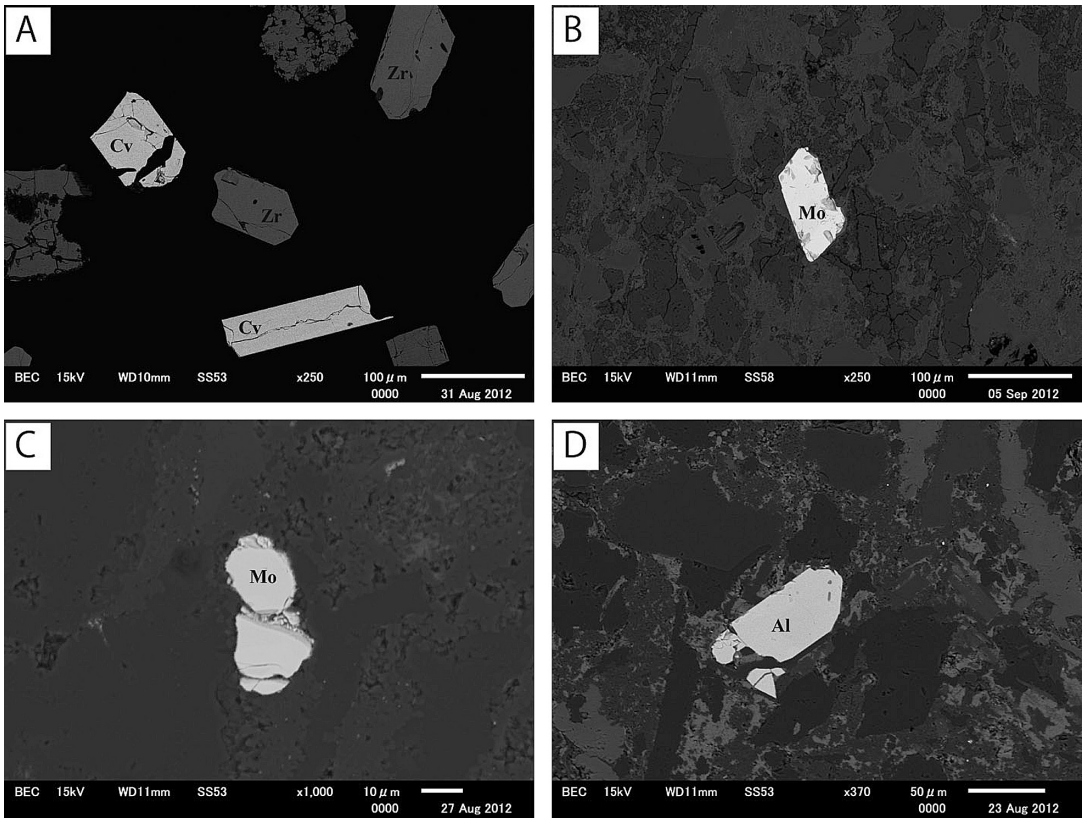

Fig. 4. Back-scattered image of chevkinite, monazite and allanite in the tuffs. A: euhedral chevkinite in a heavy fraction of the samples H-18. B: Monazite in the thin section of the samples S-5 from the Shirataki area. C: detrital monazite in the thin section of the samples H-18. D: allanite in a thin section of the samples H-21.

30–100 microns in size less than or approximately equal to quartz and plagioclase. Zircon is the most common accessory mineral in these tuffs. Several monazite grains are found in a thin section of the S-5 tuff. They are subhedral to euhedral in shape (Fig. 4B). It is considered that such monazite grains were crystallized as a phenocryst in the magma along with zircon.

In the Hegurinaka quarry, more than ten tuff layers occur. Among them, ten tuffs are observed microscopically under thin sections. In all the tuffs, quartz and plagioclase are common fragments with subordinate amounts of biotite and ilmenite, similar to those from the Shirataki area. The heavy fraction, specific gravity >3.3, of all the tuffs are collected for more detailed analyses under Energy Dispersive Spectrometry. As an accessory mineral, zircon was found in all the samples. A thin tuff, H-21 occurring at the bottom of the sequence, contains allanite as common as zircon (Fig. 4D). Chevkinite is a common mineral occurring in the heavy fractions of the thickest tuff, samples H-16 to H-18 (Fig. 4A). The mineral is confirmed even in thin section. Monazite occurs in the H-15 crystal-rich tuff. Chevkinite is found from the heavy fraction in the H-15 tuff, but is far less common than monazite. In some samples, rounded monazites are found (Fig. 4C). As a secondary mineral, calcite occurs as a vein mineral. Glauconite, chlorite, and clay minerals are also common, probably replacing mafic minerals and glass. Sulfide minerals such as pyrite and galena are present in most of the samples.

Table 1. Chemical compositions of chevkinite and monazite in the tuffs from Hegurinaka and Shirataki.

Chevkinite			Monazite							
sample No.	Hegurinaka quarry H-18		sample No.	Hegurinaka H-15		Shirataki S-5, 6		Hegurinaka quarry		
								H-18	H-18	H-18
	average	1σ		average	1σ	average	1σ	detrital	detrital	detrital
SiO_2	20.76	0.28	P_2O_5	29.38	0.56	29.20	0.65	30.11	26.48	27.93
TiO_2	18.32	0.70	SiO_2	0.46	0.12	0.71	0.21	0.59	2.83	1.91
Nb_2O_5	0.40	0.10	La_2O_3	14.24	0.78	15.68	2.20	9.73	10.00	12.18
Ta_2O_5	0.06	0.08	Ce_2O_3	30.46	0.62	30.43	1.32	24.60	27.06	31.25
Al_2O_3	0.55	0.10	Pr_2O_3	3.42	0.06	3.43	0.13	3.58	3.78	4.06
FeO	10.63	0.22	Nd_2O_3	12.00	0.24	10.85	0.68	13.43	13.92	12.96
CaO	3.02	0.39	Sm_2O_3	1.24	0.13	0.95	0.33	2.00	2.12	1.56
ThO_2	1.48	0.61	Gd_2O_3	0.96	0.12	0.75	0.34	1.69	1.48	0.72
La_2O_3	11.48	0.64	Dy_2O_3	0.29	0.06	0.26	0.20	0.26	0.52	0.22
Ce_2O_3	21.44	0.53	Y_2O_3	1.16	0.22	1.15	0.76	0.52	0.63	0.34
Pr_2O_3	2.12	0.18	UO_2	0.05	0.02	0.01	0.01	1.08	0.32	0.13
Nd_2O_3	7.57	0.36	ThO_2	5.68	0.56	4.08	1.66	9.83	11.04	7.45
Sm_2O_3	0.77	0.11	PbO	0.01	0.00	0.00	0.01	1.14	0.04	0.02
Gd_2O_3	0.41	0.30	CaO	0.85	0.11	0.92	0.44	2.17	0.06	0.03
Dy_2O_3	0.24	0.07	Total	100.20	1.12	98.40	1.29	100.74	100.29	100.77
Total	99.26	1.02	age	27 ± 9Ma		21 ± 15Ma		1874 Ma	82 Ma	73 Ma

Chemical compositions of chevkinite, monazite, and whole rock

Chemical compositions of both chevkinite and monazite were analyzed by a JEOL electron microprobe analyzer. Accelerating voltage and current were 15 KV and 20 nA for chevkinite, respectively. More detailed analyses were done for monazite age estimation which was described in detail by Santosh *et al.* (2006). The following synthetic and natural materials were used as standards: wollastonite for Si and Ca; anatase for Ti; sillimanite for Al; Mg_2SiO_4 for Mg; Fe_2SiO_4 for Fe; rhodonite for Mn; albite for Na; YP_5O_{14} for Y; LaP_5O_{14} for La; CeP_5O_{14} for Ce; PrP_5O_{14} for Pr; NdP_5O_{14} for Nd; SmP_5O_{14} for Sm; GdP_5O_{14} for Gd; DyP_5O_{14} for Dy; $FeNb_2O_6$ for Nb; $MnTa_2O_6$ for Ta; UO_2 for U; and ThO_2 for Th. Chevkinite is mostly homogeneous under back-scattered electron imaging, but monazite is sometimes a zoned crystal.

Average chemical compositions of chevkinite and monazite are shown in Table 1. The crystal structure of chevknite is described by Miyawaki *et al.* (2012). Chemical compositions of monazites from Shirataki are different in ThO_2 and UO_2 contents from those found at the Hegurinaka quarry as shown in Fig. 5. The former is depleted in UO_2, with less than 0.02 wt%, and variable in ThO_2 content, with 1 wt% to 8 wt%, whereas the latter has a narrower range of ThO_2 content, with 4 wt% to 7 wt%, and is rich in UO_2 content, 0.02 wt% to 0.08 wt%. Although age estimation for young monazite is less sensitive than the zircon age method described later, both the Shirataki and Hegurinaka monazites show average ages of 21 Ma ± 15 Ma and 28 ± 10 Ma (Table 1), respectively, which indicates a Tertiary age. Rounded grains occur in the Hegurinaka chevkinite tuff (Fig. 4C). They are 73 Ma, 82 Ma, and 1870 Ma in age (Table 1). Such old mona-

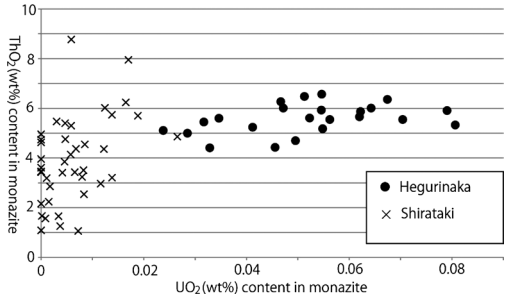

Fig. 5. Compositional variations of monazites from the tuffs at Shirataki and Hegurinaka.

zites are detritous in origin and are not a phenocryst related to Tertiary volcanism, and they were derived from the continental side.

Bulk chemical compositions of chevkinite tuff and allanite tuff from the Hegurinaka and monazite tuff from the Shirataki were obtained by the following method. They were broken in an iron mortar, sieved to 2–5 mm size chips, and washed ultrasonically- twice in alcohol and twice in distilled water. The cleaned chips were dried for ＞12 hr in an oven at 110℃ and then ground to powder in an agate mill. The powders were analyzed by X-ray fluorescence (XRF) analysis (Rigaku RIX1000) at National Museum of Nature and Science for major elements and some trace elements. Before the major element analysis, ～0.4 g of powder was weighed on a Metler Toledo dual balance system and ignited at 1025℃ for 4 hours in an electric muffle furnace to determine loss-on-ignition (LOI). Replicated analysis of several samples showed that uncertainty on LOI is 0.03 wt%. After the LOI determination, glass beads containing lithium tetraborate flux (10 to 1 dilution of sample) were prepared. For the trace elements analysis, ～4.0 g of powder was pressed into a pellet by a 12 ton force from a hydraulic press.

The bulk chemical compositions of three tuffs are listed in Table 2 in addition to that of the representative rhyolite in the Japanese Islands. The chevkinite, monazite, and allanite tuffs are higher in Ce content that the representative rhyolite. But, in spite of abundances of chevkinite and monazite in the heavy fractions, the differences are less than what was expected.

Table 2. Bulk chemical compositions of chevkinite, monazite and allanite tuffs from Hegurinaka and Shirataki.

phenocryst	Hegurinaka chevkinite	Shirataki monazite	Hegurinaka allanite	rhyolite JR-1
SiO_2 (wt%)	79.91	74.10	70.91	75.45
TiO_2	0.15	0.23	0.16	0.11
Al_2O_3	11.56	12.82	11.63	12.83
Fe_2O_3	2.18	1.88	1.53	0.89
MnO	0	0.03	0.04	0.099
MgO	0.64	0.4	0.3	0.12
CaO	0.3	0.92	3.11	0.67
Na_2O	5.02	4.04	6.16	4.02
K_2O	1.23	3.00	0.34	4.41
P_2O_5	0.03	0.09	0.04	0.021
LOI	n.d.	2.99	5.92	1.16
Total	101.02	100.50	100.14	99.78
Rb (ppm)	106	78	23	257
Ba	189	413	139	50.3
Nb	30	7.2	10.8	15.2
Pb		17	19	19.3
Sr	27	122	79	29.1
Y	101	35	45	45.1
Zr	401	175	216	99.9
Ce	144	56.5	80.8	47.2
Cr	1	7	5	2.83
Ni	22	16	14	1.67
Co	4	3	2	0.83
V	4	24	7	7
Th	17	13	15	26.7
Cu	108	46	48	2.68
Zn	146	56	90	30.6
S	118	20	281	13.3

Zircon age-LA-ICP-MS measurements

Analytical methods

The zircon grains for analysis were handpicked from heavy fractions of the Hegurinaka chevkinite tuff and Shirataki monazite tuff as well as those for SHRIMP analyses. Zircon grains from the two samples, the zircon standard FC1 ($^{206}Pb/^{238}U = 0.1859$; Paces and Miller, 1993), and NIST SRM 610 standard glass were mounted in an epoxy resin and polished until the surface was flattened with the center of the embedded grains exposed. Backscattered electron and cathodoluminescence images were used to select the sites for LA-ICP-MS analysis. After the SEM observations, the sample mount was repolished in order to remove the carbon coating and was washed with pure water in an ultrasonic bath. Height of the sample mount as well as the height of the sample holder was fixed at 5 mm to stabilize the flow of the carrier gas in the two-volume cell. This procedure is basically the same as sample preparation for SHRIMP analysis.

The experiments were carried out using LA-ICP-MS installed at the National Museum of Nature and Science. The quadrupole ICP-MS used in this study was an Agilent 7700x. The

laser ablation system was an ESI NWR213. A Nd-YAG laser with a 213 nm wavelength and 5 ns pulse were used for the machine. The operating parameters are given in Table 3. A 25 μm spot size and 4–5 J/cm^2 laser power were adopted in this study. He gas was used as the carrier gas

Table 3. ICP-MS and Laser ablation operating parameters.

ICP-MS	Agilent 7700x
Plasuma power	1350 W
Ar gas flow rate	
Prasuma	15.0 l/min
Auxiliary	0.9 l/min
Make up	0.9 l/min
He gas flow rate	590–620 ml/min
Scanning mode	Time resolved analysis
Detector mode	Pulse counting
Minitored nuclides	^{29}Si, ^{202}Hg, ^{204}Pb, ^{206}Pb, ^{207}Pb, ^{208}Pb, ^{232}Th, ^{238}U
Caliblation standard for ^{206}Pb/^{238}U ratio	FC-1 ^{206}Pb/^{238}U = 0.1859 (Paces and Miller, 1993)
Caliblation standard for U and Th consentrations and Pb isotope ratios	NIST SRM610 U: 461.5 ppm Th: 457.2 ppm ^{206}Pb/^{204}Pb = 17.051 ± 0.061 ^{207}Pb/^{206}Pb = 0.9096 ± 0.0008 ^{208}Pb/^{206}Pb = 2.1670 ± 0.0018 } (Walder *et al.*, 1993)
Laser ablation	ESI NWR213
Laser source	Nd-YAG
Wavelength	213 nm
Spot size	25 μm
Pulse energy	4–5 J/cm^2
Repetition rate	5 Hz

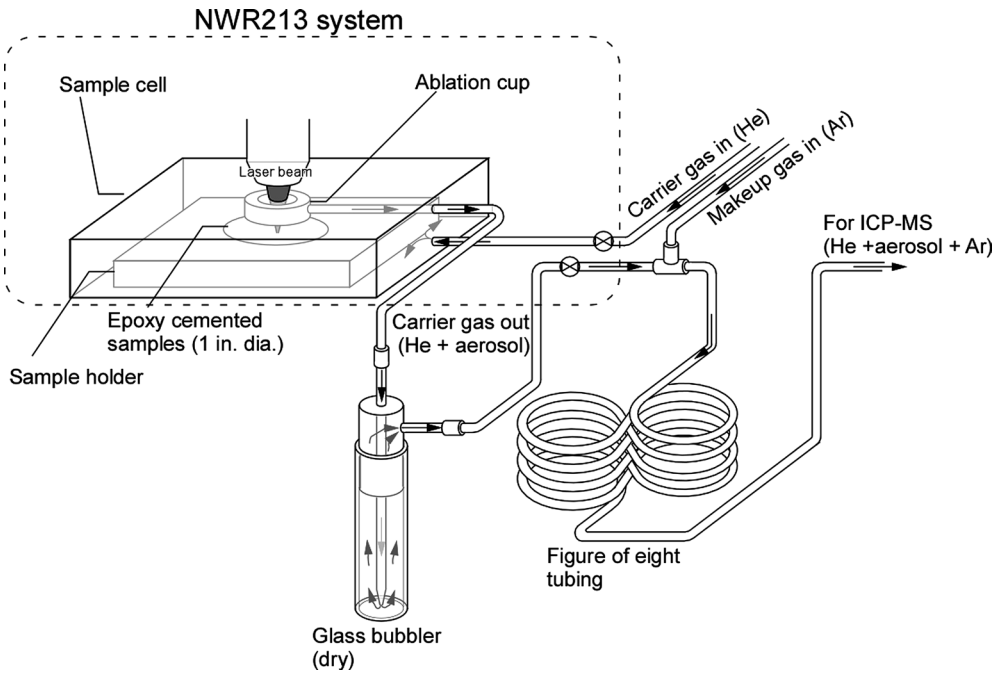

Fig. 6. Schematic diagram of the LA-ICP-MS system at National Museum of Nature and Science.

instead of Ar gas to enhance a higher transport efficiency of ablated materials (e.g. Eggins *et al.*, 1998). The flow rate of the He carrier gas and the Ar makeup gas were 580–620 ml/min. and 900 ml/min., respectively. Pure (＞99.9999 vol.%) He and Ar gases were used in this study to avoid contamination. Before each analysis, the surfaces of the samples were cleaned by shooting the laser several times in order to avoid contaminations from adhered materials. To obtain a stable profile of $^{206}Pb/^{238}U$ and Pb isotopes ratios, we attempted to attach a glass babbler between the exit of the sample cell and the junction with the Ar make-up gas. This would have an advantage similar to the stabilizer of Tunheng and Hirata (2004). Moreover, to encourage mixing between the carrier and make-up gases, the sample tube between the junction point and the ICP torch is ～2 m in length in a figure-eight configuration (Fig. 6).

All measurements were carried out using time resolved analysis. For U–Pb dating, the ^{29}Si, ^{202}Hg, ^{204}Pb (^{204}Hg), ^{206}Pb, ^{207}Pb, ^{208}Pb, ^{232}Th and ^{238}U peaks were monitored. The integration times for ^{29}Si, ^{202}Hg, ^{204}Pb (^{204}Hg), ^{208}Pb, ^{232}Th and ^{238}U were 10 ms, 30 ms for ^{206}Pb, and 40 ms for ^{207}Pb. The time for one analysis was 55 s. The first 20 s with the laser off was for the gas blank and the other 35 s for laser ablation. The total data acquisition time was 20 s in a 35 s laser ablation period because ～10 s was necessary to begin counting once the laser was turned on and the isotope ratios were stabalized.

U and Th concentrations were calibrated by using ^{29}Si as an internal calibrant and NIST SRM 610 standard glass as the reference material. Th/U ratio is calculated using calibrated concentrations of U and Th. Pb isotope ratios ($^{207}Pb/^{206}Pb$ and $^{208}Pb/^{206}Pb$) are also calibrated using NIST SRM 610 as reference material. $^{206}Pb/^{238}U$ ratios are calibrated using FC1 standard zircon. These correction factors were applied to each sample in order to correct for instrumental mass bias and time dependent elemental and isotopic fractionations. Common Pb corrections for the concordia diagrams and each age were made using ^{208}Pb and ^{207}Pb, respectively (Williams, 1998), on the basis of the model for common Pb compositions proposed by Stacey and Kramers (1975). The pooled ages presented in this study were calculated using the Isoplot/Ex software (Ludwig, 2003).

Zircon dating of chevkinite and monazite tuffs

To confirm the validity of the U–Pb age analyzed by the NMNS LA-ICP-MS, the U–Pb ages of samples that were examined by SHRIMP or TIMS were compared- Narukawa granite (87.2 ± 0.4 Ma; 1σ; Watanabe *et al.*, 2000), Otodani granodiorite (191.1 ± 0.8 Ma; 95% conf.; Horie, 2012), Hikami granite (442.0 ± 3.5 Ma; Watanabe *et al.*, 1995), AS3 (1099.0 ± 0.7 Ma; 95% conf.; Paces and Miller, 1993), and QGNG (1842.0 ± 3.1 Ma; 95% conf. Black *et al.*, 2003). The weighted mean $^{238}U–^{206}Pb^*$ ages measured by NMNS LA-ICP-MS were 86.2 ± 2.4 Ma, 189.3 ± 1.6 Ma, 442.0 ± 3.5 Ma, 1102.2 ± 8.1 Ma, and 1847 ± 13 Ma, respectively (Figs. 7 and 8). Table 4 lists zircon data of age-known samples.

Table 5 lists zircon data of tuffs from the Mineoka Belt obtained by LA-ICP-MS. All errors are 1 sigma level. Almost all zircons in the samples show rhythmic oscillatory and/or sector zoning on backscattered electron and/or cathodoluminescence images (Figs. 9 and 10) which is commonly observed in igneous zircons (Corfu *et al.*, 2003), and their higher Th/U ratios (＞0.1) also support that they are igneous in origin (Williams and Claesson, 1987; Schiøtte *et al.*, 1988; Kinny *et al.*, 1990; Hoskin and Black, 2000). Fig. 11a shows Tera–Wasserberg concordia diagram for all analyzed spots from zircons of the Hegurinaka chevkinite-bearing tuff obtained by LA-ICP-MS. All zircon age data (10 spots from 8 grains) cluster in the range from about 19.5 Ma to 22.9 Ma and the weighted mean age yields 22.1 ± 0.8 Ma (95% conf.). The zircons in Shirataki monazite tuff (28 spots from 28 grains) indicate two ages, 22.2 ± 1.5 Ma and 25.1 ± 1.6 Ma (1σ; Fig. 12). The younger age is considered to indicate the depositional age or eruption age of magma for the Shirataki tuff.

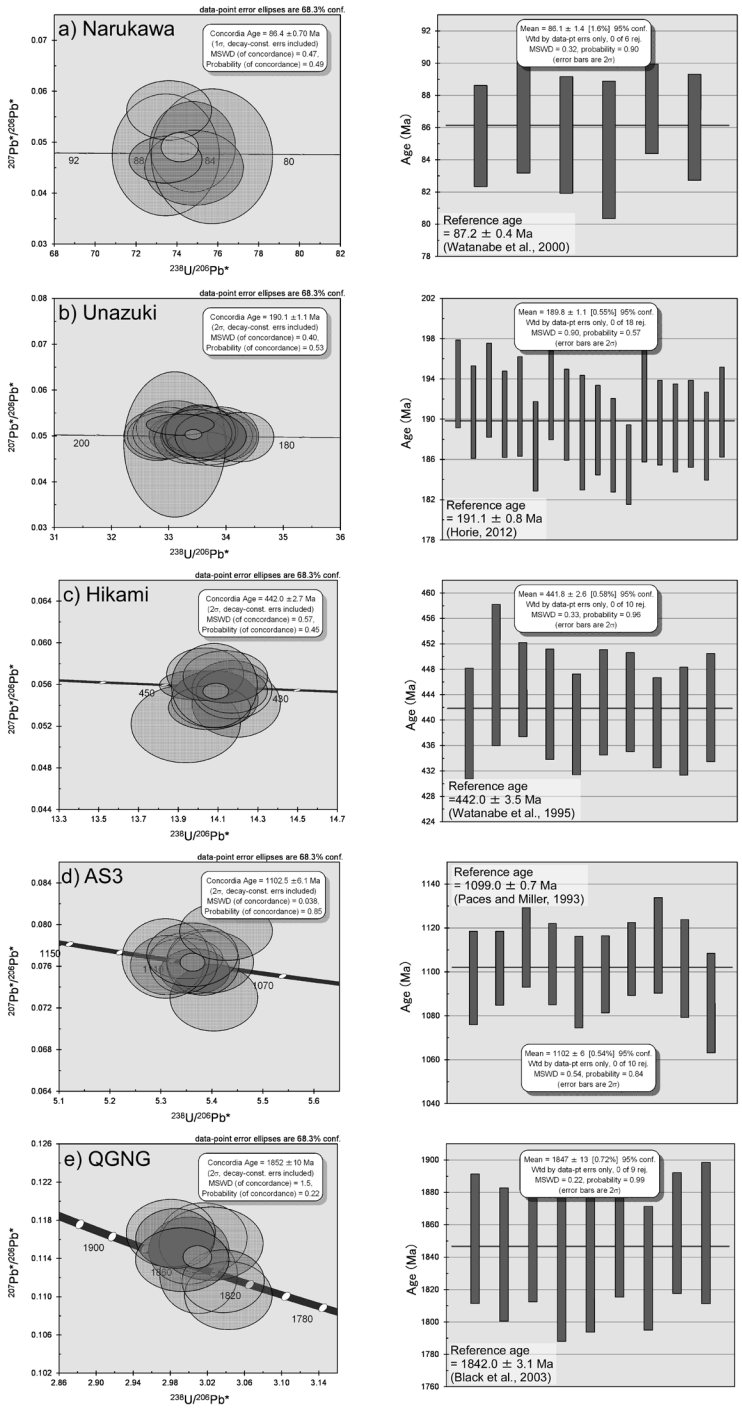

Fig. 7. Tera–Wasserburg U–Pb concordia diagrams and age distribution plot of result of LA-ICP-MS mesurements of age-known zircon samples from Narukawa Granite (a), Unazuki Granodiorite (b), Hikami Granite (c), AS3 (d) and QGNG (e). $^{207}Pb^*$ and $^{206}Pb^*$ indicate radiometric ^{207}Pb and ^{206}Pb, respectively.

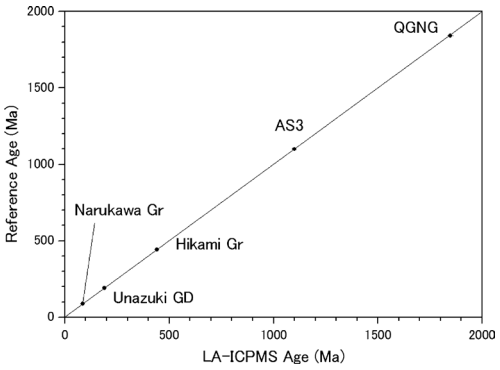

Fig. 8. Comparison of LA-ICP-MS ages determined at National Museum of Nature and Science with other reported ages.

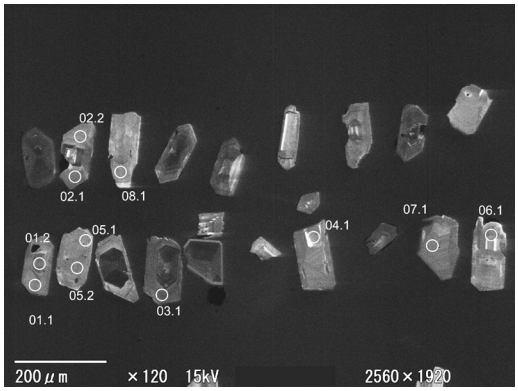

Fig. 9. Cathodoluminescence image of zircons from the Hegurinaka chevkinite-bearing tuff. Circles indicate analyzed pit by LA-ICP-MS. Numbers correspond to Table 5.

Zircon age of chevkinite-bearing tuff

SHRIMP measurement

The zircon grains for Sensitive High Resolution Ion MicroProbe (SHRIMP) analysis and the zircon standard AS3 ($^{206}Pb/^{238}U = 0.1859$; Paces and Miller, 1993) were mounted in an epoxy resin and polished. Backscattered electron and cathodoluminescence images were used to select the sites for SHRIMP analysis. U–Pb dating of the samples was carried out using the SHRIMP II installed at the National Institute of Polar Research (NIPR), Japan. The experimental conditions and the procedures followed for the measurements were based on Williams (1998). The spot size of the primary ion beam was approximately 25 μm. The U–Pb data were reduced in a manner similar to that described by Williams (1998), using the SQUID Excel macro written by Ludwig (2001). Common Pb corrections for the concordia diagrams and each Phanerozoic ages were made using ^{204}Pb and ^{207}Pb, respectively (Williams, 1998), on the basis of the model for common Pb compositions proposed by Stacey and Kramers (1975). The pooled ages presented in this study were calculated using the Isoplot/Ex software (Ludwig, 2003). The uncertainties in the mean $^{206}Pb^*/^{238}U$ ages are within the 95% confidence limits and include the uncertainty in the Pb/U calibration for each analytical session. All age data of zircons in the Hegurinaka chevkinite tuff (10 spots from 8 grains) cluster in a range from about 22.1 Ma to 23.6 Ma (Table 6) and the weighted mean age yields 22.9 ± 0.1 Ma (95% conf.; Fig. 11b).

Discussion

In the Japanese Islands, chevkinite is a scarce mineral which has previously only been reported in a granitoid from Ashizuri, Shikoku (Imaoka and Nakashima, 1994). Even though an enormous quantity of studies about volcanic ashes and tuffs in the islands have been conducted (e.g. Machida and Arai, 1992; Takahashi *et al.*, 2001), neither chevkinite nor monazite has previously been reported as a phenocryst. Such a rare mineral was found in a thick tuff layer from the Hegurinaka quarry, Boso Peninsula. Chevkinite was observed in thin section, along with zircon. Monazite is also a rare phenocryst mineral, although it was found at two localities: Hegurinaka quarry and the Shirataki area. Age of the chevkinite-bearing tuff was determined to be 22.9 ± 0.1 Ma by SHRIMP analyses and 22.1 ± 0.8 Ma by LA-ICP-MS analyses, which corresponds at the earliest to the Miocene or near the boundary between the Oligocene and Miocene similar to the results obtained by microfossils (Saito, 1992). On the other hand, monazite

Table 4. LA-ICP-MS analyzed data of age-known samples and calculated ages.

Labels	$^{206}Pb_c$ (1) (%)	U (ppm)	Th (ppm)	Th/U	$^{238}U/^{206}Pb^*$ (1)	$^{207}Pb^*/^{206}Pb^*$ (1)	$^{238}U/^{206}Pb^*$ age (1) (Ma)	$^{238}U/^{206}Pb^*$ age (2) (Ma)	$^{207}Pb^*/^{206}Pb^*$ age (1) (Ma)
Narukawa Granite									
IK01	0.11	230	71	0.32	74.73±1.39	0.0491±0.0059	85.7±1.6	85.5±1.6	—
IK02	0.20	166	70	0.43	73.42±1.73	0.0475±0.0079	87.2±2.0	87.2±2.0	—
IK03	0.00	181	88	0.50	74.81±1.59	0.0450±0.0049	85.6±1.8	85.6±1.8	—
IK04	0.28	155	68	0.45	75.68±1.96	0.0472±0.0088	84.6±2.2	84.6±2.1	—
IK05	0.00	359	210	0.60	73.40±1.18	0.0466±0.0030	87.2±1.4	87.2±1.4	—
IK06	0.00	203	138	0.69	73.59±1.37	0.0563±0.0039	87.0±1.6	86.0±1.6	—
Unazuki Granodiorite									
OT01	0.01	316	200	0.65	32.79±0.39	0.0501±0.0036	193.7±2.2	193.5±2.2	—
OT02	0.04	497	310	0.64	33.27±0.42	0.0502±0.0030	190.9±2.4	190.7±2.3	—
OT03	0.01	465	394	0.87	32.90±0.41	0.0500±0.0034	193.0±2.4	192.9±2.3	—
OT04	0.14	462	342	0.76	33.30±0.39	0.0503±0.0030	190.7±2.2	190.5±2.1	—
OT05	0.03	314	227	0.74	33.11±0.45	0.0517±0.0040	191.8±2.6	191.3±2.5	—
OT06	0.09	416	361	0.89	33.90±0.42	0.0498±0.0036	187.4±2.3	187.3±2.2	—
OT07	0.00	400	309	0.79	32.97±0.40	0.0507±0.0037	192.6±2.3	192.4±2.2	—
OT08	0.10	412	318	0.79	33.37±0.42	0.0492±0.0035	190.4±2.3	190.5±2.3	—
OT09	0.05	239	150	0.64	33.65±0.53	0.0500±0.0042	188.8±2.9	188.7±2.8	—
OT10	0.05	492	405	0.84	33.57±0.42	0.0509±0.0037	189.2±2.3	188.9±2.2	—
OT11	0.02	306	216	0.72	33.89±0.44	0.0499±0.0043	187.5±2.4	187.4±2.3	—
OT12	0.02	408	316	0.79	34.25±0.38	0.0497±0.0036	185.5±2.1	185.5±2.0	—
OT13	6.09	427	385	0.93	33.10±0.58	0.0481±0.0105	191.9±3.3	192.3±3.3	—
OT14	0.22	570	53	0.10	33.54±0.37	0.0486±0.0015	189.4±2.1	189.7±2.1	—
OT15	0.02	330	241	0.75	33.54±0.41	0.0507±0.0040	189.4±2.3	189.1±2.2	—
OT16	0.02	414	333	0.83	33.48±0.40	0.0505±0.0035	189.7±2.2	189.6±2.2	—
OT17	0.19	485	412	0.87	33.72±0.41	0.0499±0.0034	188.4±2.3	188.3±2.2	—
OT18	0.00	553	486	0.90	33.19±0.39	0.0525±0.0015	191.4±2.2	190.7±2.2	—
Hikami Granite									
HK01	0.76	677	522	0.79	14.19±0.15	0.0541±0.0021	439.0±4.4	439.5±4.3	376±88
HK02	0.17	213	70	0.34	13.94±0.18	0.0522±0.0025	446.7±5.6	447.1±5.6	294±108
HK03	0.00	859	460	0.55	13.99±0.12	0.0559±0.0009	445.2±3.7	444.8±3.7	450±37
HK04	0.28	799	454	0.58	14.08±0.14	0.0546±0.0018	442.2±4.4	442.5±4.3	395±74
HK05	0.13	394	151	0.39	14.17±0.13	0.0555±0.0019	439.6±4.0	439.4±4.0	432±75
HK06	0.03	600	187	0.32	14.06±0.14	0.0538±0.0014	443.0±4.2	442.9±4.1	361±58
HK07	0.69	771	281	0.37	14.04±0.13	0.0570±0.0017	443.7±3.9	442.9±3.9	491±65
HK08	0.04	783	344	0.45	14.17±0.12	0.0554±0.0014	439.6±3.6	439.6±3.5	427±57
HK09	0.27	428	114	0.27	14.14±0.14	0.0567±0.0017	440.6±4.2	439.9±4.2	482±64
HK10	0.03	337	217	0.66	14.08±0.14	0.0559±0.0027	442.3±4.3	442.0±4.3	448±106
AS3									
AS01	0.39	159	83	0.53	5.40±0.06	0.0730±0.0021	1094.5±10.6	1097.4±10.6	1013±58
AS02	0.12	562	393	0.72	5.37±0.04	0.0755±0.0014	1101.5±8.5	1101.8±8.4	1082±38
AS03	0.02	239	164	0.70	5.31±0.05	0.0761±0.0019	1111.9±9.1	1111.2±9.1	1098±49
AS04	0.00	248	173	0.72	5.35±0.05	0.0768±0.0013	1105.0±9.2	1103.6±9.3	1115±34
AS05	0.03	215	166	0.79	5.40±0.06	0.0764±0.0020	1095.8±10.5	1095.6±10.4	1106±51
AS06	0.03	264	227	0.88	5.38±0.05	0.0764±0.0021	1098.6±8.9	1099.1±8.8	1105±55
AS07	0.01	370	284	0.79	5.34±0.04	0.0763±0.0019	1105.7±8.4	1106.0±8.3	1103±50
AS08	0.02	142	72	0.52	5.31±0.06	0.0768±0.0025	1112.4±10.9	1112.1±10.9	1115±66
AS09	0.12	132	62	0.49	5.36±0.06	0.0771±0.0020	1102.5±11.2	1101.7±11.2	1124±52
AS10	0.00	98	36	0.38	5.43±0.06	0.0794±0.0019	1090.1±11.1	1085.9±11.3	1182±46
QGNG									
QG01	0.02	179	186	1.06	3.01±0.03	0.1123±0.0027	1849.0±14.8	1851.6±14.6	1837±43
QG02	0.00	218	238	1.12	3.02±0.03	0.1161±0.0025	1846.1±16.5	1841.8±16.2	1898±38
QG03	0.02	170	150	0.91	3.00±0.03	0.1148±0.0023	1854.6±15.4	1853.1±15.3	1877±37
QG04	0.00	189	187	1.02	3.02±0.04	0.1156±0.0025	1841.8±19.7	1835.7±19.5	1888±40
QG05	0.36	179	161	0.92	3.04±0.03	0.1101±0.0024	1831.9±16.4	1835.6±16.2	1801±39
QG06	0.00	213	240	1.16	2.98±0.03	0.1167±0.0023	1865.1±17.2	1856.8±17.0	1906±36
QG07	0.04	215	228	1.09	3.04±0.03	0.1116±0.0022	1834.9±15.4	1833.4±15.3	1826±35
QG08	0.00	252	273	1.11	2.99±0.03	0.1161±0.0021	1862.5±15.2	1855.1±15.1	1897±32
QG09	0.01	176	162	0.95	2.99±0.03	0.1139±0.0022	1858.4±18.0	1855.1±17.9	1862±35

Errors are 1-sigma; Pb_c and Pb^* indicate the common and radiogenic portions, respectively.

(1) Common Pb corrected by assuming $^{206}Pb/^{238}U$–$^{208}Pb/^{232}Th$ age-concordance

(2) Common Pb corrected by assuming $^{206}Pb/^{238}U$–$^{207}Pb/^{235}U$ age-concordance

Table 5. LA-ICP-MS U–Pb data and calculated ages of zircons in the tuff samples from the Mineoka Belt.

Labels	$^{206}Pb_c$ (1) (%)	U (ppm)	Th (ppm)	Th/U	$^{238}U/^{206}Pb^*$(1)	$^{207}Pb^*/^{206}Pb^*$(1)	$^{238}U/^{206}Pb^*$ age(1) (Ma)	$^{238}U/^{206}Pb^*$ age(2) (Ma)
Hegurinaka chevkinite-bearing tuff								
HR01.1	1.04	152	179	1.21	286.49 ± 15.32	0.0475 ± 0.0321	22.5 ± 1.2	22.4 ± 1.1
HR02.1	0.59	370	353	0.98	290.04 ± 8.88	0.0445 ± 0.0137	22.2 ± 0.7	22.2 ± 0.6
HR02.2	0.82	583	718	1.26	297.32 ± 8.42	0.0494 ± 0.0128	21.6 ± 0.6	21.6 ± 0.5
HR03.1	0.31	1135	937	0.85	289.38 ± 5.33	0.0462 ± 0.0063	22.2 ± 0.4	22.2 ± 0.4
HR04.1	0.30	291	343	1.21	291.55 ± 11.25	0.0475 ± 0.0228	22.1 ± 0.9	22.0 ± 0.7
HR05.1	1.68	142	231	1.66	298.89 ± 17.45	0.0441 ± 0.0394	21.5 ± 1.3	21.6 ± 1.1
HR05.2	10.73	167	263	1.62	306.84 ± 19.34	0.0506 ± 0.0506	21.0 ± 1.3	20.9 ± 1.0
HR06.1	0.03	273	385	1.45	290.06 ± 12.41	0.0474 ± 0.0259	22.2 ± 0.9	22.1 ± 0.8
HR07.1	0.71	278	207	0.76	296.55 ± 10.03	0.0440 ± 0.0149	21.7 ± 0.7	21.8 ± 0.7
HR08.1	2.81	162	192	1.21	280.51 ± 15.67	0.0426 ± 0.0345	22.9 ± 1.3	23.0 ± 1.0
Shirataki monazite-bearing tuff								
ST01	3.39	145	167	1.19	244.74 ± 15.03	0.0422 ± 0.0361	26.3 ± 1.6	26.4 ± 1.5
ST02	2.71	266	201	0.77	241.23 ± 11.07	0.0433 ± 0.0254	26.7 ± 1.2	26.8 ± 1.2
ST03	8.09	133	128	0.98	290.63 ± 20.51	0.0242 ± 0.0498	22.1 ± 1.6	22.8 ± 1.5
ST04	2.84	132	122	0.95	243.36 ± 14.54	0.0381 ± 0.0338	26.4 ± 1.6	26.7 ± 1.5
ST05	1.74	518	488	0.97	253.64 ± 7.58	0.0420 ± 0.0132	25.4 ± 0.8	25.5 ± 0.7
ST06	1.93	276	293	1.09	261.77 ± 11.99	0.0475 ± 0.0209	24.6 ± 1.1	24.5 ± 1.1
ST07	0.91	153	234	1.57	282.91 ± 18.20	0.0495 ± 0.0395	22.7 ± 1.5	22.6 ± 1.3
ST08	4.73	127	126	1.02	254.01 ± 17.36	0.0541 ± 0.0467	25.3 ± 1.7	25.1 ± 1.5
ST09	0.06	346	702	2.08	259.90 ± 11.39	0.0467 ± 0.0297	24.8 ± 1.1	24.7 ± 0.7
ST10	0.22	309	185	0.61	242.55 ± 8.53	0.0474 ± 0.0175	26.5 ± 0.9	26.5 ± 0.9
ST11	2.25	149	122	0.84	287.68 ± 17.06	0.0500 ± 0.0346	22.4 ± 1.3	22.2 ± 1.2
ST12	2.70	113	109	0.99	263.66 ± 18.23	0.0431 ± 0.0444	24.4 ± 1.7	24.5 ± 1.6
ST13	0.32	727	567	0.80	249.23 ± 5.87	0.0489 ± 0.0093	25.8 ± 0.6	25.7 ± 0.6
ST14	0.59	567	433	0.78	258.59 ± 6.25	0.0452 ± 0.0098	24.9 ± 0.6	24.9 ± 0.6
ST15	1.98	113	100	0.91	273.11 ± 17.95	0.0425 ± 0.0443	23.6 ± 1.5	23.7 ± 1.5
ST16	0.49	344	293	0.87	254.84 ± 7.37	0.0470 ± 0.0140	25.2 ± 0.7	25.2 ± 0.7
ST17	18.99	159	151	0.98	278.77 ± 24.11	0.0558 ± 0.0796	23.1 ± 2.0	22.8 ± 1.7
ST18	2.10	168	145	0.88	282.62 ± 14.43	0.0406 ± 0.0318	22.8 ± 1.2	22.9 ± 1.1
ST19	4.36	164	163	1.02	287.88 ± 14.91	0.0528 ± 0.0347	22.4 ± 1.2	22.2 ± 1.1
ST20	1.69	248	329	1.36	267.70 ± 12.27	0.0408 ± 0.0263	24.0 ± 1.1	24.2 ± 0.9
ST21	3.58	106	70	0.68	292.14 ± 20.69	0.0567 ± 0.0387	22.0 ± 1.6	21.7 ± 1.5
ST22	4.90	147	154	1.07	261.14 ± 17.31	0.0406 ± 0.0503	24.6 ± 1.6	24.8 ± 1.4
ST23	3.74	131	108	0.84	260.79 ± 16.30	0.0468 ± 0.0394	24.7 ± 1.5	24.7 ± 1.5
ST24	1.20	112	96	0.88	250.96 ± 15.47	0.0475 ± 0.0381	25.6 ± 1.6	25.5 ± 1.5
ST25	16.15	104	75	0.74	297.76 ± 22.14	0.0407 ± 0.0647	21.6 ± 1.6	21.7 ± 1.6
ST26	1.69	127	114	0.92	286.06 ± 17.45	0.0453 ± 0.0340	22.5 ± 1.4	22.5 ± 1.3
ST27	3.06	98	74	0.78	278.11 ± 21.21	0.0462 ± 0.0486	23.1 ± 1.8	23.1 ± 1.6
ST28	7.32	267	502	1.93	274.71 ± 14.13	0.0484 ± 0.0377	23.4 ± 1.2	23.3 ± 0.9

Errors are 1-sigma; Pb_c and Pb^* indicate the common and radiogenic portions, respectively.

(1) Common Pb corrected by assuming $^{206}Pb/^{238}U$–$^{208}Pb/^{232}Th$ age-concordance

(2) Common Pb corrected by assuming $^{206}Pb/^{238}U$–$^{207}Pb/^{235}U$ age-concordance

tuff from the Shirataki area shows two ages of 22.2 ± 1.5 Ma and 25.1 ± 1.6 Ma by LA-ICP-MS. The younger age should be the depositional age of the tuff, but the older age is probably due to accidental fragments derived from the wall rock or cap rock at an eruption. The mixture of essential and accidental fragments is not uncommon in ash and tuff (e.g. Yokoyama *et al.*, 1997). The age 22.2 ± 1.5 Ma for the tuff is consistent with results by planktonic foraminifers in the associated limestone-chert sequence (Mohiuddin and Ogawa, 1996).

The Mineoka Belt at the southern part of the Boso Peninsula is composed of many tectonic blocks which are not continuous with each other. Although microfossil ages of sedimentary rocks in the tectonic blocks are relatively narrow in range from the Eocene to early Miocene, isotope ages of whole rock and minerals, mostly determined by the K–Ar method, are variable from 14 Ma to

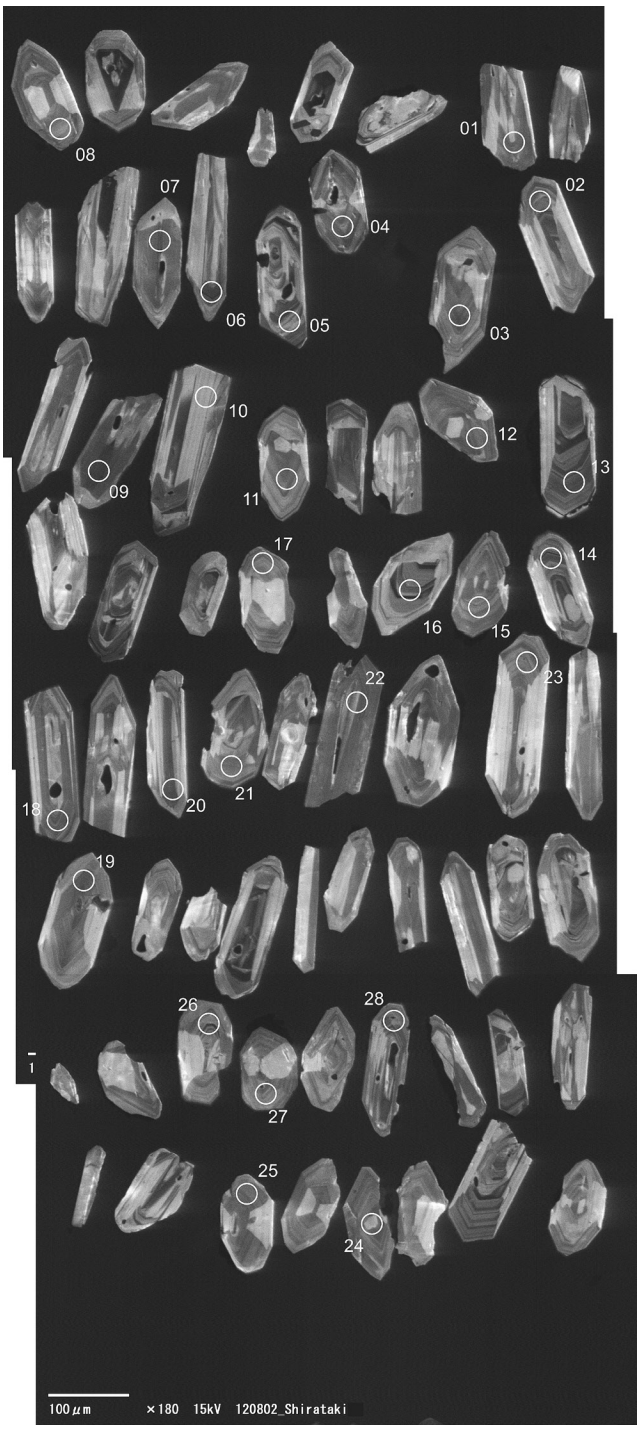

Fig. 10. Cathodoluminescence image of zircons from Shirataki monazite-bearing tuff. Circles indicate analyzed pit by LA-ICP-MS. Numbers correspond to Table 5.

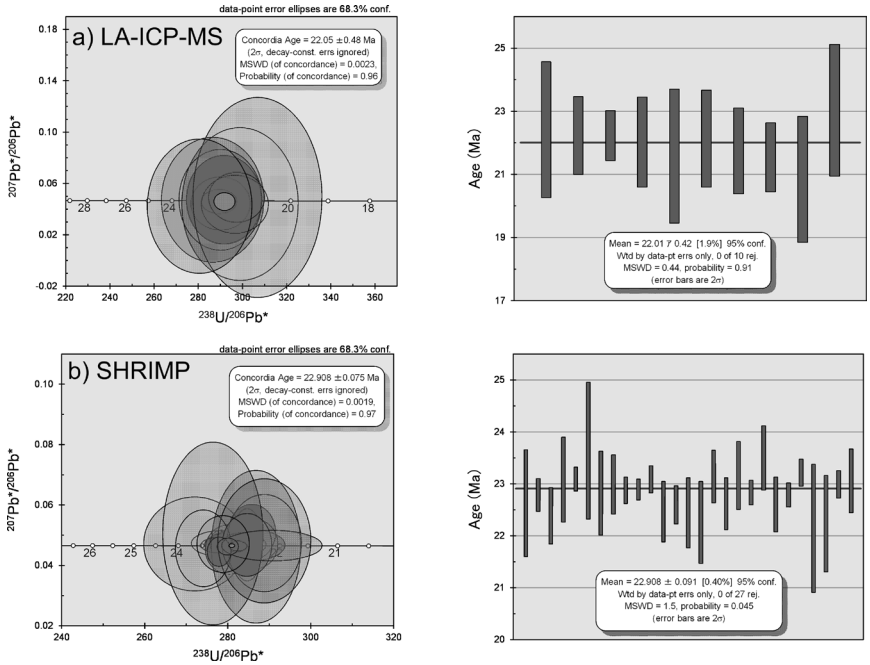

Fig. 11. Tera–Wasserburg U–Pb concordia diagrams and age distribution plot of Hegurinaka tuff sample analyzed by LA-ICP-MS (a) and SHRIMP (b) $^{207}Pb^*$ and $^{206}Pb^*$ indicate radiometric ^{207}Pb and ^{206}Pb, respectively.

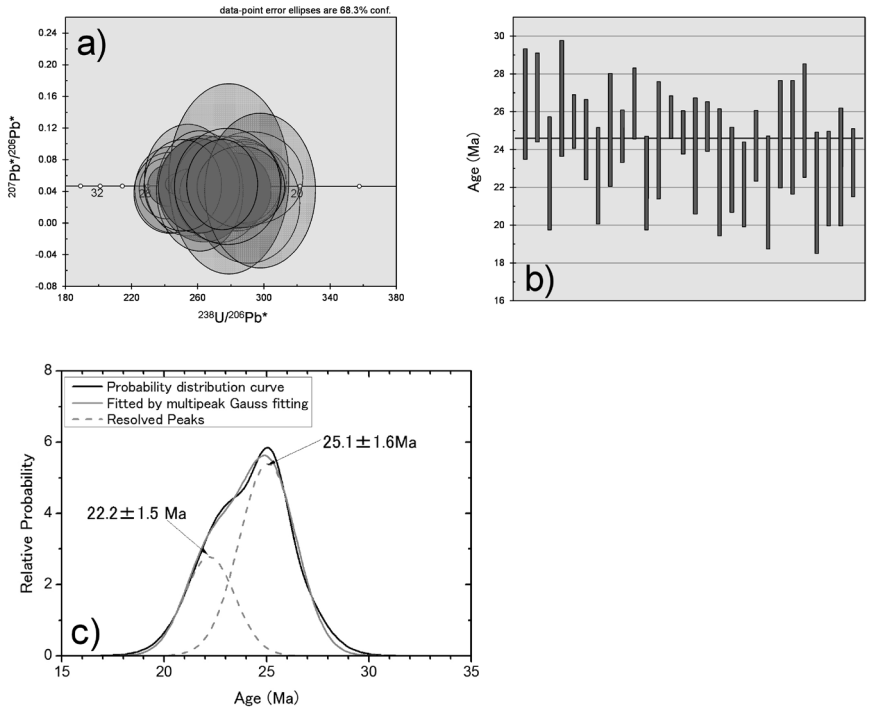

Fig. 12. Tera–Wasserburg U–Pb concordia diagram (a), age distribution plot (b) and age distribution diagram (c) of Hegurinaka tuff sample analyzed by LA-ICP-MS. $^{207}Pb^*$ and $^{206}Pb^*$ indicate radiometric ^{207}Pb and ^{206}Pb, respectively. The zircons in the Shirataki tuff is composed with two age components; 22.2 ± 1.5 Ma and 25.1 ± 1.6 Ma (1σ).

Table 6. SHRIMP U–Pb data and calculated ages of the Hegurinaka chevkinite-bearing tuff sample from the Mineoka Belt.

Labels	$^{206}Pb_c$ (1) (%)	U (ppm)	Th (ppm)	Th/U	$^{238}U/^{206}Pb^*$ (1)	$^{207}Pb^*/^{206}Pb^*$ (1)	$^{238}U/^{206}Pb^*$ age (1) (Ma)	$^{238}U/^{206}Pb^*$ age (2) (Ma)
KY1-01.1	0.00	83	562	2.30	284.24 ± 6.33	0.0466 ± 0.0036	22.6 ± 0.5	22.6 ± 0.5
KY1-02.1	0.35	791	216	0.73	282.43 ± 1.99	0.0462 ± 0.0019	22.8 ± 0.2	22.8 ± 0.2
KY1-02.2	1.76	273	150	0.82	285.77 ± 3.79	0.0510 ± 0.0061	22.5 ± 0.3	22.4 ± 0.3
KY1-04.1	0.00	108	1352	0.99	278.50 ± 4.84	0.0472 ± 0.0028	23.1 ± 0.4	23.1 ± 0.4
KY1-05.1	0.00	1549	271	0.90	278.66 ± 1.37	0.0463 ± 0.0007	23.1 ± 0.1	23.1 ± 0.1
KY1-06.1	2.99	115	226	2.45	271.93 ± 8.07	0.0471 ± 0.0103	23.7 ± 0.7	23.6 ± 0.7
KY1-07.1	0.00	124	191	1.88	281.78 ± 4.89	0.0468 ± 0.0028	22.8 ± 0.4	22.8 ± 0.4
KY1-08.1	1.14	221	1774	0.89	280.30 ± 3.80	0.0453 ± 0.0054	23.0 ± 0.3	23.0 ± 0.3
KY1-08.2	0.42	1164	1649	1.57	281.16 ± 1.56	0.0467 ± 0.0013	22.9 ± 0.1	22.9 ± 0.1
KY1-09.1	0.55	1911	1012	0.89	281.08 ± 1.25	0.0463 ± 0.0013	22.9 ± 0.1	22.9 ± 0.1
KY1-10.1	0.16	1077	164	0.97	278.40 ± 1.82	0.0472 ± 0.0029	23.1 ± 0.2	23.1 ± 0.1
KY1-11.1	2.24	206	1513	0.82	286.20 ± 3.85	0.0470 ± 0.0055	22.5 ± 0.3	22.5 ± 0.3
KY1-12.1	1.66	1735	202	0.90	284.60 ± 2.49	0.0468 ± 0.0079	22.6 ± 0.2	22.6 ± 0.2
KY1-13.1	3.28	169	109	1.24	286.77 ± 7.08	0.0462 ± 0.0167	22.4 ± 0.6	22.4 ± 0.3
KY1-14.1	3.13	112	320	1.01	288.71 ± 5.94	0.0473 ± 0.0107	22.3 ± 0.5	22.3 ± 0.4
KY1-15.1	0.00	360	273	0.92	277.97 ± 2.99	0.0466 ± 0.0017	23.1 ± 0.2	23.1 ± 0.3
KY1-16.1	0.00	323	136	0.88	283.84 ± 3.07	0.0482 ± 0.0018	22.7 ± 0.2	22.6 ± 0.2
KY1-17.1	0.07	187	1910	0.75	276.33 ± 7.96	0.0505 ± 0.0201	23.3 ± 0.7	23.2 ± 0.3
KY1-17.2	0.29	2395	312	0.82	281.80 ± 1.51	0.0463 ± 0.0014	22.8 ± 0.1	22.8 ± 0.1
KY1-18.1	1.36	282	286	1.14	274.07 ± 4.45	0.0456 ± 0.0084	23.5 ± 0.4	23.5 ± 0.3
KY1-19.1	1.40	262	1469	1.13	284.56 ± 3.95	0.0467 ± 0.0069	22.6 ± 0.3	22.6 ± 0.3
KY1-20.1	0.32	1860	1037	0.82	282.38 ± 1.44	0.0464 ± 0.0011	22.8 ± 0.1	22.8 ± 0.1
KY1-21.1	0.39	1265	162	0.85	277.86 ± 1.88	0.0444 ± 0.0032	23.2 ± 0.2	23.2 ± 0.1
KY1-22.1	0.00	83	366	2.00	290.54 ± 8.01	0.0465 ± 0.0034	22.1 ± 0.6	22.1 ± 0.6
KY1-23.1	2.42	123	950	3.08	288.78 ± 7.40	0.0481 ± 0.0136	22.3 ± 0.6	22.2 ± 0.5
KY1-24.1	0.47	1173	243	0.84	279.94 ± 1.67	0.0462 ± 0.0018	23.0 ± 0.1	23.0 ± 0.1
KY1-25.1	0.18	247	30	1.02	278.83 ± 4.19	0.0470 ± 0.0062	23.1 ± 0.3	23.1 ± 0.3

Errors are 1-sigma; Pb_c and Pb^* indicate the common and radiogenic portions, respectively.

(1) Common Pb corrected using measured ^{204}Pb.

(2) Common Pb corrected by assuming $^{206}Pb/^{238}U$–$^{207}Pb/^{235}U$ age-concordance.

94 Ma. It is usually inevitable when using the K–Ar age technique to discuss the alteration or metamorphism of each sample. On the other hands, zircon is an ultrastable mineral that is not easily metamorphosed or altered, as closure temperature of zircon is more than 900°C. With the SHRIMP and LA-ICP-MS methods, many zircon grains are analyzed, and then multiple events can be discussed from complex age data. Age by SHRIMP or LA-ICP-MS cannot be obtained from a zircon-free sample. However, the age data obtained from zircons are the most plausible and contribute to the geotectonic reconstruction of the blocks in the Mineoka Belt very well.

Chevkinite and monazite tuffs from the Boso Peninsula are specific to the Japanese Islands. They were formed at the latest Oligocene to Early Miocene. The Japanese Islands are mostly composed of rocks older than Oligocene and younger than Early Miocene. Geological formations showing the Oligocene–Miocene boundary is rare on the islands (e.g. Geological Survey of Japan, 2011), and mostly occurs along the Sea of Japan (e.g. Yoshikawa *et al.*, 2002; Ozaki *et al.*, 2006; Kano *et al.*, 2011). Siliceous volcanic rocks with ages of 20–30 Ma developed in the formations along the coast and they are usually terrigenous in origin and formed just before the opening of the Sea of Japan at 20–15 Ma. The chevkinite-bearing tuff contains monazite with an age of 1874 Ma clearly derived from the continental side. Although details on heavy mineral

and age analyses of the volcanic rocks are necessary to pursue their provenance, the coastal zone of the Sea of Japan is one of the most probable candidates for the provenance of the chevkinite and monazite tuffs.

Ackowledgement

We would like to thank Prof. Z. Yang for his helpful reviews.

References

Black, L. P., Kamo, S. L., Williams, I. S., Mundil, R., Davis, D. W., Korsch, R. J. and Foudoulis, C. (2003) The application of SHRIMP to Phanerozoic geochronology; a critical appraisal of four zircon standards. *Chemical Geology*, **200**: 171–188.

Corfu, F., Hanchar, J. M., Hoskin, W. O. and Kinny, P. (2003) An atlas of zircon textures. In: Hanchar, J. M. & Hoskin, W. O. (Eds.), *Zircon: Reviews in Mineralogy and Geochemistry 53*, pp. 278–286. Mineralogical Society of America, Washington D.C.

Das K., Yokoyama K., Chakraborty P. P. and Sarkar A. (2009) Basal tuff contemporaneity of Chattisgarh and Khariar basins, based on new dates and geochemistry. *Journal of Geology,* **117:** 88–102.

Eggins, S. M., Kinsley, L. P. J. and Shelley, J. M. G. (1998) Deposition and element fractionation processes of occurring during atmospheric pressure sampling for analysis by ICP-MS. *Applied Surface Science*, **129**: 278–286.

Geological Survey of Japan, AIST (Ed.). (2011) Seamless digital geological map of Japan 1: 200,000. Research Information Database DB084, Geological Survey of Japan, National Institute of Advanced Industrial Science and Technology.

Hirano, N., Ogawa, Y., Saito, K., Yoshida, T., Sato, H. and Taniguchi, H. (2003) Multi-stage evolution of the Tertiary Mineoka ophiolite, Japan: new geochemical and age constraints. *Geological Society*, London, Special publications, **218**: 279–298.

Hiroi, Y. (1995) Metamorphic block in the Kamogawa Harbor. In: Natural History Museum and Institute, Chiba (Eds.), *Natural Reserve Report for Geology and Minerals: Report from Chiba Prefecture, Japan*. pp. 105. Education Board of Chiba Prefecture, Chiba, Japan. (In Japanese.)

Horie, K. (2012) U–Pb geochronological map of Unazuki area. *Abstracts of Japan Geoscience Union Meeting 2012*, SGL43-P09.

Hoskin, P. W. and Black, L. P. (2000) Metamorphic zircon formation by solid-state recrystallization of protolith igneous zircon. *Journal of Metamorphic Geology*, **18**: 423–439.

Imaoka, T. and Nakashima K. (1994) Chevkinite in syenites from Cape Ashzuri, Shikoku island, Japan. *Neues Jahrbuch für Mineralogie abhandlungen*, **8**: 358–366.

Izett, G. A. and Wilcox, R. E. (1968) Perrierite, chevkinite, and allanite in upper Cenozoic ash beds in the western United States. *American Mineralogist*, **53**: 1558–1567.

Kano, K., Ogguchi, T., Yanagisawa, Y., Awata, Y., Kobayashi, N., Sano, Y., Hayashi, S., Kitazato, H., Ogasawara, K. and Komazawa, M. (2011) Geology of the Toga and Funakawa district. Quadrangle Series, 1:50,000. Geological Survey of Japan. AIST, 127P. (In Japanese with English abstract.)

Kinny, P. D., Wijbrans, J. R., Froude, D. O., Williams, I. S. and Compston, W. (1990) Age constraints on the geological evolution of the Narryer Gneiss Complex, Western Australia. *Australian Journal of Earth Sciences*, **37**: 51–69.

Ludwig, K. R. (2001) SQUID version: 1.03—A user's manual. Berkeley Geochronology Center Special Publication No. 2, pp. 19–xxx, Berkeley Geochronology Center, Berkeley, CA., USA.

Ludwig, K. R. (2003) User's manual for Isoplot 3.00. A geochronological toolkit for Microsoft Excel. Berkeley Geochronology Center Special Publication No. 4, pp. 70–xxx, Berkeley Geochronology Center, Berkeley, CA., USA.

Macdonald R., Bagiński B., Kartashov P., Zozulya D. and Dzierżanowski P. (2012) Chevkinite-group minerals from Russia and Mongolia: new compositional data from metasomatites and ore deposits. *Mineralogical Magazine*, **76**: 535–549.

Machida, H. and Arai, F. (1992) Atlas of tephra in around japan. University of Tokyo Press, pp. 276–xxx. (In Japanese.)

Mitchell, R. S. (1966) Virginia metamict minerals: perrierite and chevkinite. *American Mineralogist*, **51**: 1394–1405.

Mitsunashi, T., Kikuchi, T., Suzuki, Y., Hirayama, J., Nakajima, T., Oka, S., Kodama, K., Horiguchi, M., Katsurajima, S., Miyashita, M., Yazaki, K. and Kageyama, K. (1979) The geology of Tokyo Bay and its adjacent areas. Geological Survey of Japan. Miscellaneous map serried, 20. (In Japanese with English abstract.)

Miyawaki, R., Matsubara, S., Yokoyama, K., Monma, K., Sano, T., Shigeoka, M and Nishikubo, K. (2012) Chevkinite-(Ce) in tuff at Heguri, Boso Peninsula, Chiba Prefecture, Japan. *Bulletin of the National Museum of nature and Science*, **38**: 7–13.

Muhiuddin, M. M. and Ogawa, Y. (1996) Middle Eocene to early Oligocene planktonic foraminifers from the

micritic limestone beds of the Heguri area, Mineoka Belt, Boso Peninsula, Japan. *Journal of the Geological Society of Japan*, **102**: 611–617.

Muhiuddin, M. M. and Ogawa, Y. (1998a) Early Miocene pelagic sequences in the Mineoka Belt, Boso Peninsula, Japan. *Journal of the Geological Society of Japan*, **104**: 1–12.

Muhiuddin, M. M. and Ogawa, Y. (1998b) Late Paleocene-middle Miocene pelagic sequences in the Boso Peninsula: new light on northwest Pacific tectonics. *The Island Arc*, **7**: 301–314.

Ozaki, M., Imaoka, T. and Ikawa, T. (2006) Geology of the Senzaki district. Quadrangle Series, 1:50,000. Geological Survey of Japan. AIST, 127P. (In Japanese with English abstract.)

Paces, J. B. and Miller, J. D. (1993) Precise U–Pb ages of Duluth Complex and related mafic intrusions, northeastern Minnesota: geochronological insights to physical, petrogenetic, paleomagnetic, and tectonomagmatic processes associated with the 1.1 Ga midcontinent rift system. *Journal of Geophysical Research*, **98**: B8, 13997–14013.

Platt, R., Wall, F., Williams, C. T. and Woolley. R. A. (1987) Zirconolite, chevkinite and other rare earth minerals from nepheline syenite and peralkaline granites and syenites of Chilwa Alkaline Province, Malawi. *Mineralogical Magazine,* **51**: 253–263.

Saito, S. (1992) Stratigraphy of Cenozoic strata in the southern terminus area of Boso Peninsula, Central Japan. Contribution of Institute of Geology and Palaeontology, Tohoku University, **93**: 1–37. (In Japanese with English abstract.)

Santosh, M., Morimoto, T., and Tsutsumi, Y. (2006) Geochronology of the khondalite belt of Trivandrum Block, Southern India: electron probe ages and implications for Gondwana tectonics. *Gondwana Research*, **9**: 261–278.

Schiøtte, L., Compston, W. and Bridgwater, D. (1988) Late Archaean ages for the deposition of clastic sediments belonging to the Malene supracrustals, southern West Greenland: evidence from an ion probe U–Pb zircon study. *Earth and Planetary Science Letters*, **87**: 45–58.

Sokolova E. V., Hawthorne F. C., Della Ventura, G. and Kartashov, P. M. (2004) Chevkinite-(Ce): crystal structure and the effect of moderate radiation-induceddamage on site-occupancy refinement. *Canadian Mineralogist*, **42**: 1013–1025.

Stacey, J. S. and Kramers, J. D. (1975) Approximation of terrestrial lead isotope evolution by a two-stage model. *Earth and Planetary Science Letters*, **26**: 207–221.

Takahashi, N. (1994) Alkali basalt-clastic sequence in the western end of the Mineoka Belt, Boso Peninsula, Japan. Journal of the Natural History Museum and Institute, Chiba, **3**: 1–18. (In Japanese with English abstract.)

Takahashi, N., Mitsuoka, T. and Yokoyama, K. (2001) Correlation of tuffs occurring near the boundary between Tertiary and Quaternary in the central part of the Boso Peninsula and Choshi area, Central Japan. *Memoir of National Science Museum, Tokyo*, **37**: 21–34.

Tunheng, A. and Hirata, T. (2004) Development of signal smoothing device for precise elemental analysis using laser ablation-ICP-mass spectrometry. *Journal of Analytical Atomic Spectrometry*, **19**: 932–934.

Watanabe, T., Fanning, C. M., Uruno, K. and Kano, H. (1995) Pre-Middle Silurian granitic megmatism and associated metamorphism in northern Japan: SHRIMP U–Pb zircon chronology. *Geological Journal*, **30**: 273–280.

Watanabe, T., Ireland, T., Tainosho, Y. and Nakai, Y. (2000) Zircon U–Pb sensitive high mass-resolution ion microprobe dating of granitoids in the Ryoke metamorphic belt, Kinki District, Southwest Japan. *The Island Arc*, **9**: 55–63.

Williams, I. S. (1998) U-Th-Pb geochronology by ion microprobe. In Applications of Microanalytical Techniques to Understanding Mineralizing Processes (McKibben M. A., Shanks C. P. and Ridley W. I. Ed.), *Reviews in Economic Geology*, **7**, Society of Economic Geologists, Littleton, CO, 1–35.

Williams, I. S. and Claesson, S. (1987) Isotopic evidence for the Precambrian provenance and Caledonian metamorphism of high grade paragneisses from the Seve Nappes, Scandinavian Caledonides. *Contributions to Mineralogy and Petrology*, **97**: 205–217.

Yokoyama, K., Mitsuoka, T. and Takahashi, N. (1997) Reconnaissance of modal proportions and chemical compositions of heavy minerals in tuffs from the Boso Peninsula, Central Japan. *Bulletin of National Science Museum*, Tokyo, **23**: 61–77.

Yokoyama, K., Tsutsumi, Y., Nhung, N. T. and Quynh, P. V. (2010) Age distribution of monazits from the nine rivers of Vietnam. *Memoir of National Museum of Nature and Science*, **46**: 97–108.

Yoshida, Y. (1974) Finding of foraminifers from the Mineoka Hill, Chiba Prefecture. *Chishitunyuusu,* **233**: 30–36. (In Japanese.)

Yoshikawa, T., Kano, K., Yanagisawa, Y., Komazawa, M., Joshima, M. and Kikawa, E. (2002) Geology of the Suzumisaki, Noto-iida and Horyuzan district. Quadrangle Series, 1:50,000. Geological Survey of Japan. AIST, 76P. (In Japanese with English abstract.)